

Cell-free biogenesis of bacterial division proto-rings that can constrict liposomes

Godino, Elisa; López, Jonás Noguera; Zarguit, Ilias; Doerr, Anne; Jimenez, Mercedes; Rivas, Germán; Danelon, Christophe

DOI

[10.1038/s42003-020-01258-9](https://doi.org/10.1038/s42003-020-01258-9)

Publication date

2020

Document Version

Final published version

Published in

Communications Biology

Citation (APA)

Godino, E., López, J. N., Zarguit, I., Doerr, A., Jimenez, M., Rivas, G., & Danelon, C. (2020). Cell-free biogenesis of bacterial division proto-rings that can constrict liposomes. *Communications Biology*, 3(1), Article 539. <https://doi.org/10.1038/s42003-020-01258-9>

Important note

To cite this publication, please use the final published version (if applicable).
Please check the document version above.



Copyright

Other than for strictly personal use, it is not permitted to download, forward or distribute the text or part of it, without the consent of the author(s) and/or copyright holder(s), unless the work is under an open content license such as Creative Commons.

Takedown policy

Please contact us and provide details if you believe this document breaches copyrights.
We will remove access to the work immediately and investigate your claim.

Cell-free biogenesis of bacterial division proto-rings that can constrict liposomes

Elisa Godino¹, Jonás Noguera López¹, Ilias Zarguit¹, Anne Doerr¹, Mercedes Jimenez ², Germán Rivas² & Christophe Danelon ¹✉

A major challenge towards the realization of an autonomous synthetic cell resides in the encoding of a division machinery in a genetic programme. In the bacterial cell cycle, the assembly of cytoskeletal proteins into a ring defines the division site. At the onset of the formation of the *Escherichia coli* divisome, a proto-ring consisting of FtsZ and its membrane-recruiting proteins takes place. Here, we show that FtsA-FtsZ ring-like structures driven by cell-free gene expression can be reconstituted on planar membranes and inside liposome compartments. Such cytoskeletal structures are found to constrict the liposome, generating elongated membrane necks and budding vesicles. Additional expression of the FtsZ cross-linker protein ZapA yields more rigid FtsZ bundles that attach to the membrane but fail to produce budding spots or necks in liposomes. These results demonstrate that gene-directed protein synthesis and assembly of membrane-constricting FtsZ-rings can be combined in a liposome-based artificial cell.

¹Department of Bionanoscience, Kavli Institute of Nanoscience, Delft University of Technology, van der Maasweg 9, 2629HZ Delft, The Netherlands. ²Centro de Investigaciones Biológicas Margarita Salas, CSIC, 28040 Madrid, Spain. ✉email: c.j.a.danelon@tudelft.nl

Cell-free biology aims at understanding cellular processes by reconstituting biological functions from their isolated elementary components in *in vitro* model systems. Owing to their openness and easy manipulation, cytoplasmic extracts and systems reconstituted from purified elements are more amenable to customized experimental design and quantitative description compared to living cells. Therefore, the minimal requirements to achieve a particular function can be assessed more reliably. Many complex biological structures and processes taking place in bacterial or eukaryotic cells have already been reconstituted *in vitro*. Notable achievements include the reconstitution of the minimal translation machinery from *Escherichia coli*¹, the yeast DNA replication apparatus², filopodial structures³, cytoskeleton self-organization and centrosome positioning⁴, egg cytokinesis signaling⁵, DNA segregation with Par⁶, and clathrin-coated buds⁷. Encouraged by the many cellular pieces that have already been reconstituted *in vitro*, synthetic biologists have now engaged in the construction of an entire cell^{8–12}.

One of the hallmarks of living systems is their ability to divide. An obvious starting point to conceiving a biology-inspired division mechanism in artificial cells is to consider the canonical pathways taking place in prokaryotes. In most bacteria, symmetrical cell division proceeds by forming a constriction ring that eventually splits the mother cell into equally sized daughter cells¹³. At an earlier stage of cytokinesis, a proto-ring composed of the FtsZ, FtsA, and ZipA proteins, assembles on the inner leaflet of the cytoplasmic membrane at the future division site^{14–16}. The tubulin-related FtsZ is the core constituent of the proto-ring. FtsZ is a GTPase that can polymerize into protofilaments^{17,18}. Anchoring of FtsZ protofilaments to the cytoplasmic membrane is mediated by ZipA and the actin homolog FtsA^{19–21}. This process is regulated by accessory proteins belonging to the Zap family²².

Earlier attempts to divide cell-like liposomal compartments have focused on the reconstitution of the Z-ring from purified proteins^{23,24}. These studies have shown that FtsZ aided by one of its anchoring protein partners—or a chimeric FtsZ bearing a membrane targeting segment²⁵—can self-organize into filament patterns on supported lipid membranes^{25–28}. When encapsulated inside vesicles, the elementary cytoskeletal proteins form ring-like structures that can deform the liposome membrane^{24,29,30}. Whether FtsZ filaments alone exert a contractile force and contribute to the final stage of division remains a subject of debate^{31,32} and evidence for complete liposome division is still lacking.

A conceptual issue that is inherent to reconstitution assays solely relying on purified proteins, is the impossibility to maintain steady amounts of cytoskeletal proteins from internal mechanisms as the compartment undergoes division. Another problem raised by conventional cell-free assays is the use of oversimplified buffer compositions that have been tailored for a particular set of enzymatic reactions but fail to reproduce the cytoplasmic environment.

Herein, we address these issues by encoding *E. coli* division proteins on DNA templates. Genetic control over protein production offers a general solution to achieve self-replication, as well as self-regulation by establishing feedback loops. In this context, the PURE system, a minimal gene expression system reconstituted primarily from *E. coli* constituents¹ was employed. Different types of proteins and biological functions have already been synthesized *de novo* with the PURE system, including membrane-associated proteins^{10–12,33}. Moreover, by containing all relevant factors for gene expression, the PURE system emulates more closely the molecular composition of the bacterial cytoplasm than simple buffers. In the present study we utilized PURE_{frex2.0}, which provides the best combination of protein yield and expression lifespan^{34,35}.

We show that cell-free expressed FtsA is able to recruit FtsZ polymers, forming large-scale two-dimensional networks of curved and ring-like structures in the absence of bundling factors. When the entire set of reactions is encapsulated inside liposomes, proto-rings of FtsA-FtsZ filaments are found to constrict the vesicle, generating extended membrane necks and budding vesicles, a phenotype that has not been reported before. Co-expression of ZapA, a native stabilizer of FtsZ filaments, yields stiffer FtsZ bundles attached to the membrane that fail to constrict into bud necks. FtsZ cytoskeletal structures are also investigated with ZipA membrane-anchor protein. We find that in our low-volume supported lipid bilayer (SLB) assays with ZipA and $\leq 3 \mu\text{M}$ FtsZ, the generic crowding agent Ficoll70 is necessary to elicit bundle formation. Cell-free expressed ZapA obviates the need of Ficoll70 and promotes formation of cytoskeletal networks with different, likely more physiological, morphology, and protein monomer dynamics. The prospects of further improvement suggest that the DNA-programmed hierarchical assembly of the Z-ring in liposomes is a promising strategy for dividing synthetic cells. In addition, our approach to reconstituting cellular processes in PURE system provides a generic platform that fills the gap between classical *in vitro* and in cellulo experiments.

Results

Cell-free synthesized FtsA drives the formation of curved FtsZ filaments. An essential component of the *E. coli* division proto-ring is FtsA, a homolog of actin that anchors FtsZ filaments to the cytoplasmic membrane. To bypass the difficult purification of FtsA²⁸, we directly expressed a sequence-optimized *ftsA*_{opt} gene on an SLB (Fig. 1a). In the presence of $3 \mu\text{M}$ purified FtsZ-A647, curved filaments and dynamic ring-like structures formed on the membrane (Fig. 1b, Supplementary Fig. 1, Supplementary Note 1, Movie 1), concurring with previous reports^{12,28}.

To obtain quantitative insights about the concentration of cell-free synthesized FtsA, pre-ran PURE system samples were analyzed by liquid chromatography-coupled mass spectrometry (LC-MS) (Supplementary Fig. 2, Supplementary Table 1). Protein abundance was quantified using an internal standard (QconCAT) for the most C-terminal peptide detected. We deduced that, after 3 h of expression, FtsA concentration on the SLB was $2.2 \pm 0.2 \mu\text{M}$ (mean \pm SD, three biological repeats) (Fig. 1a–d, Supplementary Tables 2 and 3), corresponding to a protein ratio [FtsZ]:[FtsA] $\approx 1.5:1$. *In vivo*, FtsA concentration is $\sim 0.5 \mu\text{M}$ and the protein ratio [FtsZ]:[FtsA] = $3:1$ – $5:1$ ³⁶. However, overlapping rings and dynamic filaments on a lipid membrane have also been observed at protein ratios similar as in our cell-free assay^{26,28}. Note that LC-MS data do not report the concentration of active protein, which may differ from the measured concentration of proteolytic peptides.

Promoting lateral interactions of FtsZ protofilaments stimulates the formation of higher-order cytoskeletal structures *in vitro*³⁷. However, little is known about how the nature of these lateral interactions influences the morphology of the FtsZ network. Therefore, we decided to investigate the architecture and dynamics of FtsZ protofilaments in a molecular environment that favors lateral interactions. First, we employed Ficoll70, a generic crowding agent known to elicit FtsZ bundle formation (Fig. 1c). Large SLB areas were covered with curved filaments, rings of different sizes (most having a diameter of 1–2 μm , phenotype 1) and large circular patterns (phenotype 2) (Fig. 1d).

Although Ficoll70 is commonly used as a macromolecular crowder to mimic cytoplasmic conditions^{24,33,38,39}, we reasoned that ZapA, an *in vivo* regulator of FtsZ polymerization, would provide a more targeted and native mechanism to elicit lateral interaction, thus conferring physiologically relevant properties of

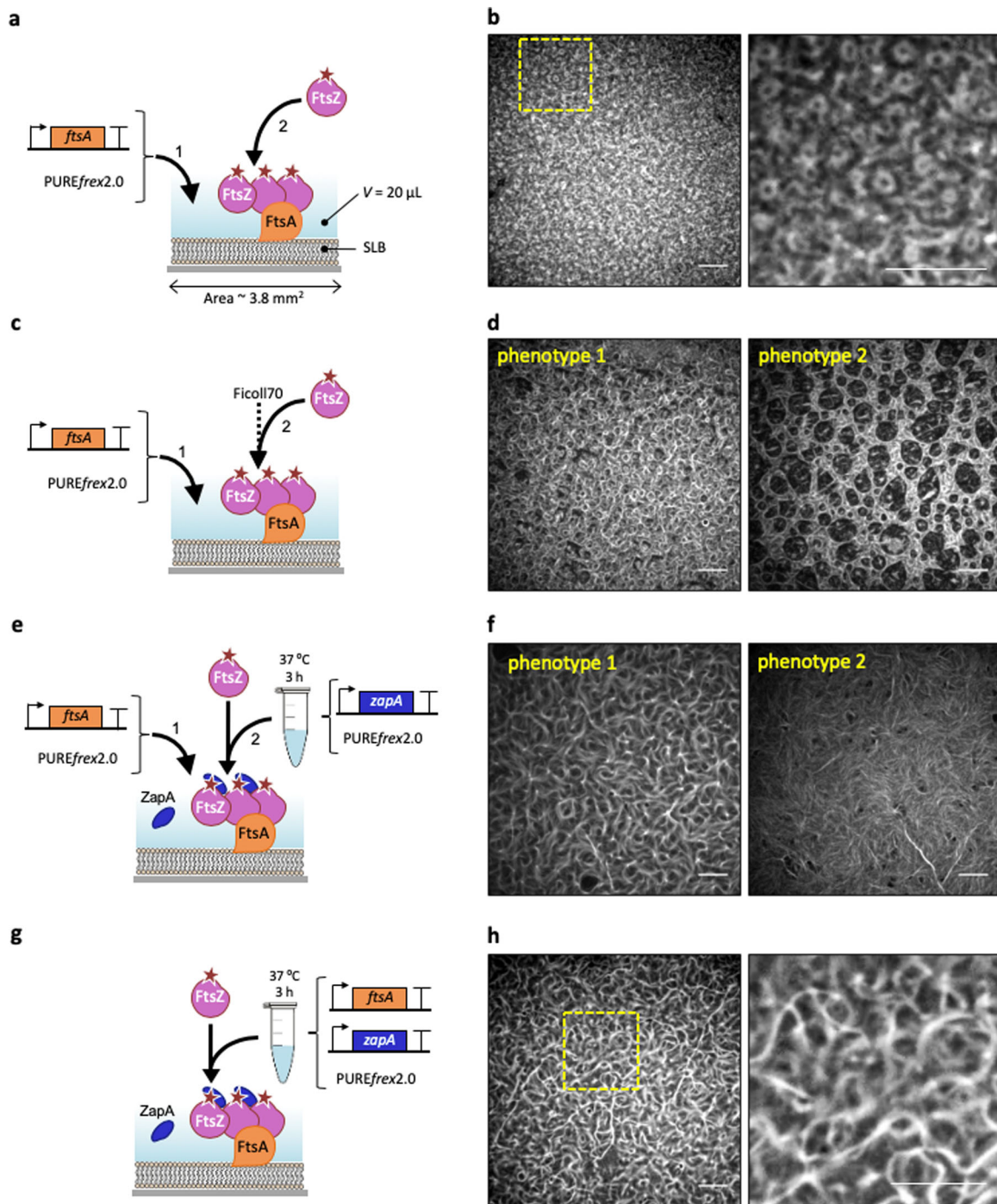


Fig. 1 Cell-free expressed FtsA recruits FtsZ to an SLB and drives the formation of ring-like structures. **a** Schematic representation of the SLB assays with FtsA directly expressed on the membrane. Purified FtsZ-A647 (3 μ M) was added. The sequence-optimized construct *ftsA_{opt}* was used. **b** Fluorescence image of FtsZ-A647 forming curved filaments and rings in the presence of in situ synthesized FtsA. The zoom-in image (right) corresponds to the framed region in the left image. **c** As in (**a**) but the solution was supplemented with Ficoll70. **d** Fluorescence image of FtsZ-A647 forming curved filaments and rings in the presence of in situ synthesized FtsA and Ficoll70. Two representative filament network morphologies observed on the same SLB are shown, phenotype 1 being the most prominent. **e** Schematic illustration of the SLB assays with separately expressed FtsA and ZapA. The constructs *ftsA_{opt}* and *zapA* were used. Purified FtsZ-A647 (3 μ M) was included. **f** Fluorescence images of FtsZ-A647 displaying two representative phenotypes from different regions of the same SLB, phenotype 1 being the most prominent. **g** Schematic illustration of the SLB assays with co-expressed FtsA and ZapA from *ftsA_{opt}* and *zapA_{opt}* constructs. Purified FtsZ-A647 (3 μ M) was added. **h** Fluorescence images of FtsZ-A647. The zoom-in image (right) corresponds to the framed area in the left image. Scale bars indicate 10 μ m.

cytoskeletal patterns. For this reason, ZapA was produced in PURE $_{\text{frex2.0}}$ starting from its native gene sequence. Substitution of Ficoll70 with cell-free synthesized ZapA produced curved bundles but also long and straight filaments of FtsZ-A647 recruited to the membrane by cell-free synthesized FtsA (Fig. 1e, f). The concentration of cell-free synthesized ZapA in the SLB assay was estimated by LC-MS to be $0.2 \pm 0.1 \mu\text{M}$ (mean \pm SD, three biological repeats, Supplementary Table 3), which is significantly lower than in *E. coli* ($1.5 \mu\text{M}$)⁴⁰. Remarkably, even at such a low concentration, ZapA is able to reshape FtsZ protofilaments (Fig. 1f).

Quantitative image analysis revealed that both the curvature and occurrence of branching points of the filament network were reduced in the presence of either Ficoll70 or ZapA (Supplementary Fig. 3b). Differences between the two phenotypes observed in each condition were also quantified (Supplementary Fig. 3c). We speculate that local changes, such as protein concentration (e.g., owing to edge effects in the chamber) and possible defects in the membrane, may play a role in the nucleation, morphology, or dynamics of the cytoskeletal network, therefore driving formation of one versus the other phenotype on the same SLB.

We challenged the PURE system to co-express both FtsA and ZapA in a single reaction. Given the low amount of ZapA produced in a single-gene reaction and the extra burden imposed on the biosynthesis machinery when expressing an additional gene, we attempted to boost ZapA concentration by substituting the native gene with a sequence-optimized *zapA*_{opt} DNA construct (Supplementary Fig. 4). Co-expression of the *ftsA*_{opt} and *zapA*_{opt} genes in a one-pot PURE system reaction led also to the formation of bended and straight bundles (Fig. 1g, h, Supplementary Fig. 5) that qualitatively resemble phenotype 1 obtained in separate expression (Fig. 1e, f). Protein quantification was performed by LC-MS, and concentration values of $2.4 \pm 0.3 \mu\text{M}$ FtsA and $0.4 \pm 0.2 \mu\text{M}$ ZapA in the SLB assay were determined (mean \pm SD, three biological repeats, Supplementary Table 3). Quantitative inspection of the protein patterns in co-expression experiments shows a lower curvature and branch point density than in single-gene expression assays (Supplementary Fig. 3b), which may be attributed to higher protein concentrations on the SLB when FtsA and ZapA are co-expressed (Supplementary Table 3). Note again that LC-MS data do not provide an accurate measure of the concentration of active protein. Furthermore, usage of PURE system substrates and cofactors, such as the tRNAs and NTPs, is different in a single-gene or double-gene expression (e.g., nucleotide and codon abundance), which may influence reactions not directly involved in transcription/translation.

Despite morphological differences observed in the protein patterns between the Ficoll70- and ZapA-containing samples, quantitative analysis of FtsZ subunit dynamics by fluorescence recovery after photobleaching (FRAP) revealed similar recovery half-time values under the tested conditions (Supplementary Fig. 6).

Bundling enables long sZipA-FtsZ cytoskeletal structure formation. We then examined the self-organization of FtsZ with the membrane-anchor soluble ZipA (sZipA) using purified proteins supplied in a minimal buffer or in PURE $_{\text{frex2.0}}$ background. The soluble variant sZipA does not contain the transmembrane region by elimination of the hydrophobic N-terminal domain (amino acids 1–25) of the full-length protein. This domain was substituted by a His₆-tag for binding NTA-conjugated lipids. The FtsZ-binding properties of sZipA are essentially the same as those of the native protein when incorporated in nanodiscs^{41,42}. We found that in our low-volume SLB assays with $\leq 3 \mu\text{M}$ FtsZ, filament bundling with either Ficoll70 or ZapA was required to trigger large-scale

cytoskeletal networks (Fig. 2a, b, Supplementary Note 2). This result contrasts with previous observations^{20,28}, highlighting the role of the total reaction volume as a control parameter in the formation of cytoskeletal patterns. The network morphology, as well as the sZipA and FtsZ monomer dynamics differ whether lateral interactions are promoted by the artificial molecular crowder Ficoll70 or by cell-free synthesized ZapA (Fig. 2c–f, Supplementary Figs. 7–11). Moreover, we found that increasing the expression level of ZapA (Supplementary Fig. 4) results in more stable filaments that can even extend above the SLB (Supplementary Figs. 8 and 9). Taken together, our results show that ZapA encourages the formation of membrane-bound sZipA-FtsZ filament network having a different—presumably more physiological—morphology and subunit turnover compared with Ficoll70.

We conclude from these SLB experiments that short, curved filaments and rings that resemble physiological structures are more prominent with FtsA compared with sZipA, and can develop in the absence of a bundling agent.

FtsZ and internally synthesized FtsA constrict liposomes. The identification of FtsZ and FtsA as the minimal molecular set to obtain membrane-anchored curved filaments and rings in the PURE system prompted us to reconstitute FtsA-FtsZ cytoskeletal networks inside liposomes (Fig. 3a). The cell-free gene expression solution was supplemented with adenosine triphosphate (ATP, additional 2 mM), guanosine triphosphate (GTP, additional 2 mM) and a mixture of highly purified chaperones (DnaK mix). Although energy regeneration components are present in the PURE system, extra ATP and GTP were provided to compensate for the extra demand from FtsA and FtsZ. Purified FtsZ-A647 was used to visualize protein localization by laser scanning confocal microscopy. FtsZ-A647 was employed at $3 \mu\text{M}$ concentration, which is similar to that measured in vivo ($\sim 3.5 \mu\text{M}$)³⁶. Liposomes were formed by natural swelling, with a composition of zwitterionic PC and PE phospholipids, anionic PG and cardiolipin, and a small fraction of TexasRed-conjugated lipid for membrane imaging³⁵. Such a lipid mixture and liposome preparation method have proved compatible with the cell-free synthesis of membrane-associated enzymes¹⁰, DNA replication proteins¹¹ and division proteins¹². Liposome size distribution ranges from $\sim 1 \mu\text{m}$ up to over $15 \mu\text{m}$ in diameter, which provides a more relevant bacterial cell-size compartment than $>20 \mu\text{m}$ liposomes produced with other methods^{23,33}. In contrast with previous studies³³, no crowding agent was included during liposome formation. In fact, we found that Ficoll70 impairs formation of gene-expressing liposomes with our methodology (Supplementary Fig. 12).

In control experiments where the *ftsA*_{opt} gene was omitted, FtsZ was exclusively located in the liposome lumen (Supplementary Fig. 13). De novo synthesized FtsA successfully recruited FtsZ on the membrane as shown by the colocalization of the FtsZ-A647 and membrane dye signals (Fig. 3, Supplementary Fig. 14). Although homogeneous recruitment of FtsZ to the membrane was commonly found within the liposome population, the majority of the liposomes displayed regions with patches of FtsZ on the inner surface of the membrane (Fig. 3b). Noticeably, the membrane spots with clustered FtsZ coincide with different types of membrane remodeling. In some cases, the recruited FtsZ localizes with outward membrane deformation or short protrusions (Fig. 3c, Supplementary Fig. 15). In other instances, the protrusions developed into vesicles or blebs tethered to the parental liposome through a membrane neck coated with FtsZ (Fig. 3d, Supplementary Fig. 15). Sometimes, the budding neck extends over a few microns in the form of a tubular structure containing one or a few FtsA-FtsZ rings (Fig. 3d, e). Interestingly,

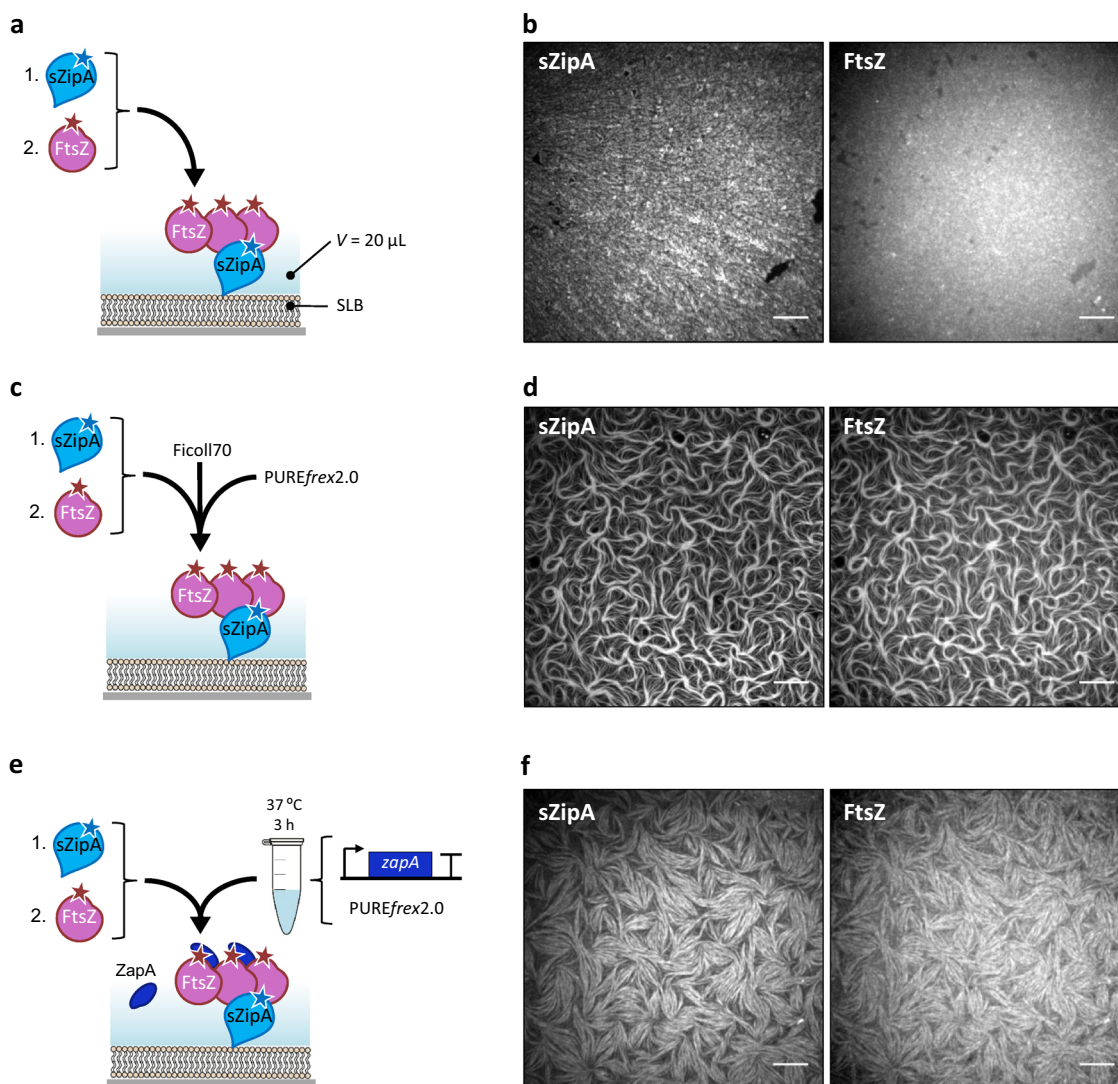


Fig. 2 Purified sZipA and FtsZ form co-filament networks in the PURE system. **a** Schematic representation of the SLB assays. Purified sZipA-A488 was first incubated on an SLB. The solution on top of the SLB was replaced by a minimal reaction buffer containing 3 μM purified FtsZ-A647 and 2 mM GTP. **b** Fluorescence images of sZipA-A488 (left) and FtsZ-A647 (right) in the minimal reaction buffer without Ficol70. **c** Schematic representation of the SLB assays. Purified sZipA-A488 was first incubated on an SLB. The solution on top of the SLB was replaced by PUREflex2.0 supplemented with 3 μM purified FtsZ-A647, 2 mM GTP and 50 g L⁻¹ Ficol70. **d** Fluorescence images of sZipA-A488 (left) and FtsZ-A647 (right) in PUREflex2.0 with Ficol70. Large-scale filaments with colocalizing FtsZ-A647 and sZipA-A488 are exclusively observed in the presence of Ficol70. This conclusion is valid in both the minimal reaction buffer and in PUREflex2.0 background. More fields of view are displayed in Supplementary Fig. 7. **e** Schematic illustration of the SLB assays with purified FtsZ-A647 (3 μM) and cell-free synthesized ZapA incubated on top of an sZipA-A488-bound SLB. ZapA was expressed from the native gene *zapA*. **f** Fluorescence images of sZipA-A488 (left) and FtsZ-A647 (right) in a sample containing cell-free synthesized ZapA and additional 2 mM GTP. Different cytoskeletal network phenotypes were observed when ZapA concentration was increased upon expression of the optimized *zapA_{opt}* construct (Supplementary Fig. 9). Scale bars indicate 10 μm.

these blebbing structures are dynamic. Events, such as appearance of new constriction sites, growing vesicles and diffusion of protein rings along the tube axis were observed (Fig. 3e, Movie 2). Although membrane recruitment of FtsZ in the form of patches was visible already within 2 h of expression, major liposome-remodeling events, such as budding spots and elongated blebs were observed only after 3–4 h. Moreover, after 6 h expression, small vesicles were found to agglutinate to larger liposomes (Supplementary Fig. 13). FtsA concentration does not significantly increase beyond the first 3 h of expression (Supplementary Fig. 2), in agreement with the kinetic profiles of protein production with the PURE system³⁴. Concentration of synthesized FtsA was compared after 3 and 6 h expression, yielding $4.5 \pm 0.5 \mu\text{M}$ and $5.8 \pm 1.1 \mu\text{M}$, respectively. Therefore, we do not

expect that the differences observed at incubation times longer than 3 h can be attributed to an increase in protein concentration. Instead, the time-dependent changes could be due to some delaying factors, such as recruitment of proteins to the membrane, assembly of filaments and bundles, protein clustering into patches and remodeling of the membrane. It is unclear whether the FtsZ-coated membrane necks can close to release mature vesicles. Therefore, we cannot ascertain that the small vesicles observed after 6 h are reminiscent to division events. Yet, these aggregated vesicles were not observed when the *ftsA_{opt}* gene was omitted (Supplementary Fig. 13), indicating that this global remodeling is dependent on the expression of FtsA.

We then decided to investigate how the presence of cell-free expressed ZapA would modulate the properties of the cytoskeletal

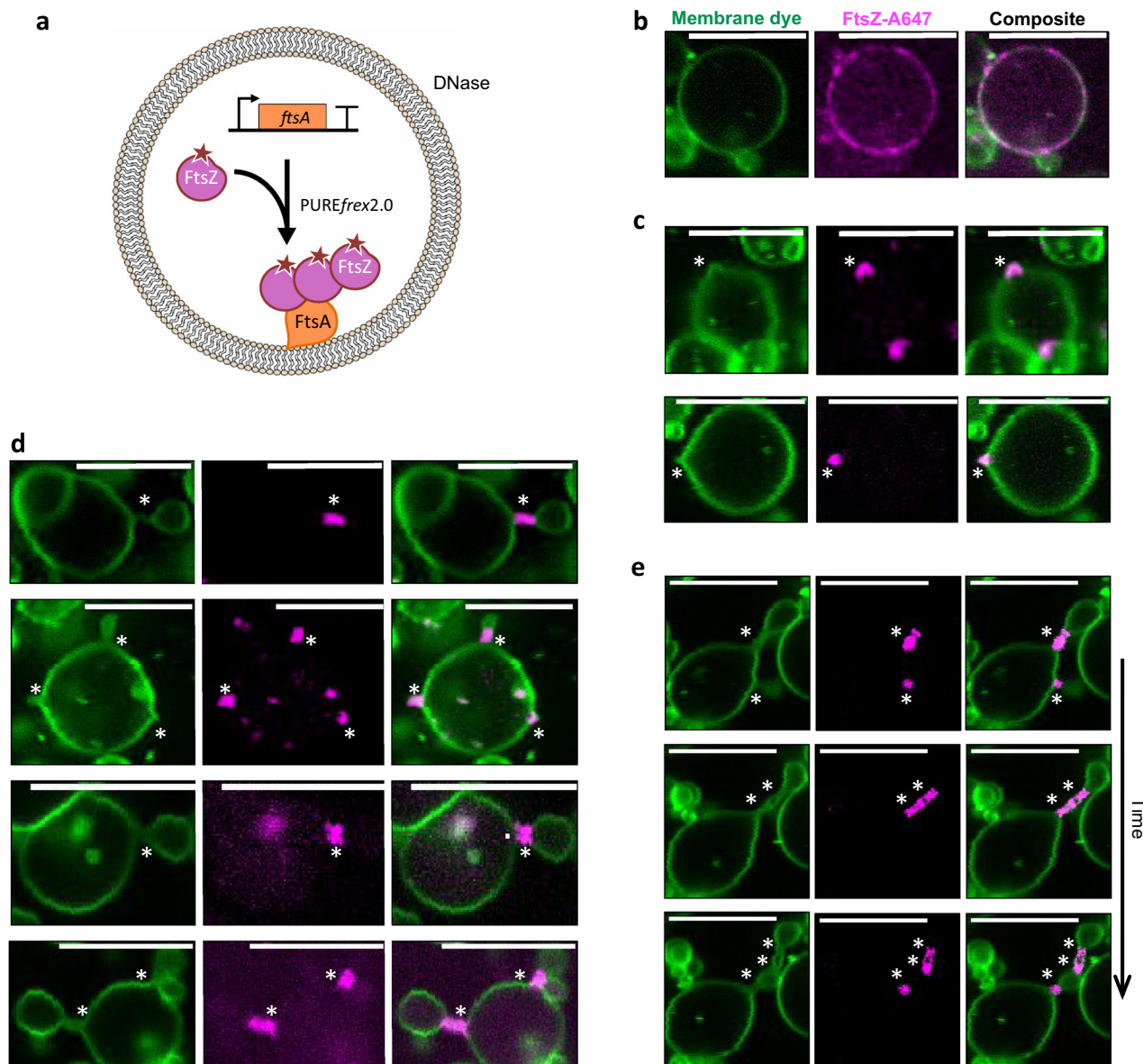


Fig. 3 In-liposome synthesized FtsA assemblies with FtsZ into ring-like structures that drive vesicle budding. **a** Schematic illustration of liposome reconstitution assays. The *ftsA_{opt}* DNA template was expressed within phospholipid vesicles in the presence of 3 μ M purified FtsZ-A647. **b–d** Confocal fluorescence images of liposomes exhibiting different morphologies of FtsZ-FtsA cytoskeletal structures and membrane remodeling: recruitment of proteins to the membrane in the form of clusters with no visible membrane deformation **b**, budding spots induced by local accumulation of FtsZ-FtsA **c**, and budding vesicles from a parental liposome with a clear FtsA-FtsZ-coated membrane neck **d**. **e** Time series images showing that a ring-forming protein cluster localized at a constriction site can split, which induces multiple necks separated by blebbing vesicles (see Movie 2). Timespan is 120 s between the first and second row of images, and 96 s between the second and third row. Fluorescence from the membrane dye is colored in green and FtsZ-A647 signal is in magenta. The composite image is the overlay of the two channels. Asterisks indicate budding spots or constriction sites. Scale bars represent 10 μ m. More examples of liposomes are shown in Supplementary Figs. 14 and 15.

patterns in liposomes (Fig. 4a). Co-expression of *ftsA_{opt}* and *zapA_{opt}* DNA constructs induced formation of FtsZ-A647 clusters on the inner surface of the membrane (Fig. 4b). Liposomes with different cytoskeletal protein phenotypes were observed, such as homogeneous coating to the membrane, patches or filaments, and large ring-like structures. Bundles of FtsZ polymers adopting apparent ring-like structures predominantly localize at the interface of two liposomes (Fig. 4b), coinciding with a membrane septum (i.e., a membrane separating two adjacent vesicles; it could be a single bilayer or two bilayers). However, ZapA abolishes the formation of membrane protrusions, vesicle budding and clustering of FtsZ on tubular membrane structures (Fig. 4b). We have seen that, in the

presence of ZapA, the small ring-like structures do not form on SLB, where longer, curved filaments dominate (Fig. 1). We observed a decrease of the filament curvature in the presence of ZapA, especially during co-expression of FtsA and ZapA (Supplementary Fig. 3b), which correlates with a higher concentration of ZapA in the assay (Supplementary Table 3). The straighter cytoskeletal filaments are likely not able to develop into contractile rings. Instead, they accommodate to the large compartment and are unable to deform the membrane into narrow necks (Fig. 4b). These results indicate that the mechanical properties of FtsZ-ZapA bundles impede the formation of membrane-constricting, high-curvature cytoskeletal filaments, which suggests that temporal

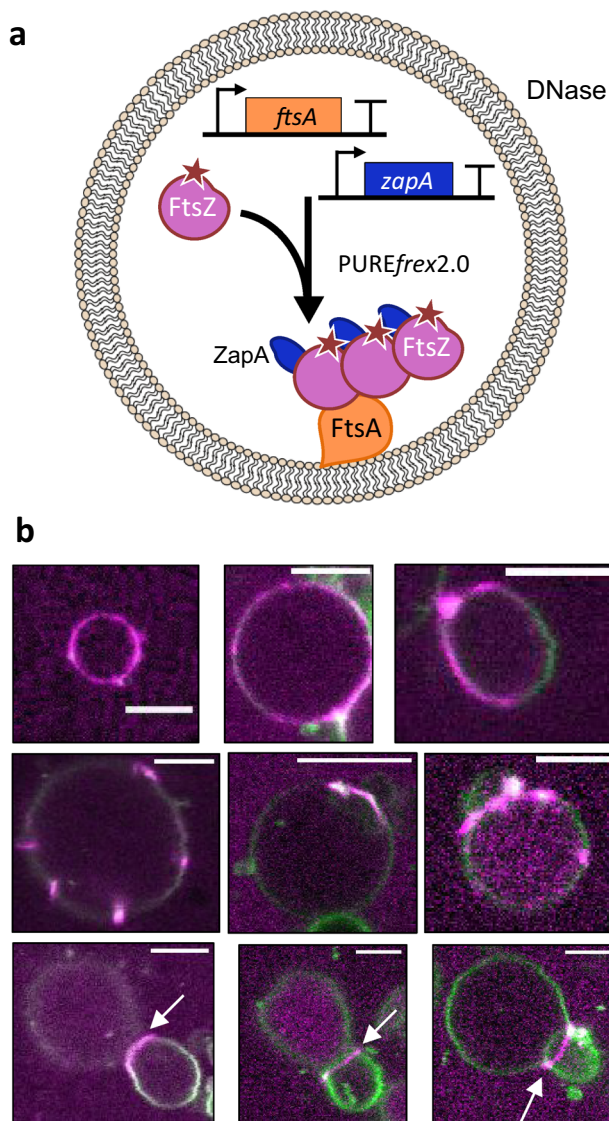


Fig. 4 Co-expressed FtsA and ZapA organize FtsZ into long membrane-tethered bundles within liposomes. **a** Schematic illustration of liposome reconstitution assays with 3 μm purified FtsZ-A647 and co-expression of the *ftsA*_{opt} and *zapA*_{opt} DNA constructs. **b** Confocal fluorescence images of liposomes exhibiting membrane recruitment of FtsZ-A647 after 3 h incubation. Fluorescence from the membrane dye is colored in green and FtsZ-A647 signal is in magenta. Only the composite images are displayed. Arrows indicate membrane septa with co-localized FtsZ. Scale bars represent 5 μm .

regulation of the local concentration of ZapA might play a role in the constriction of the FtsZ ring.

Collectively, the results demonstrate that gene-based reconstitution of membrane-constricting cytoskeletal protein filaments within liposomes is feasible. Moreover, FtsA and FtsZ form the minimal architecture to establish *E. coli* cell division proto-rings from native constituents *in vitro*.

Discussion

Compartmentalization of PURE system and of the Z-ring constituents inside liposomes provides a realistic cellular environment. Purified FtsZ and FtsA proteins have already been enclosed within small (diameter < 200 nm) liposomes³⁰ or giant vesicles⁴³. In these earlier studies, membrane-tethered proto-filaments of FtsZ could assemble with FtsA*, a mutant of FtsA

that cannot polymerize^{44,45}. In another report, the FtsZ-sfGFP fusion protein was recruited to the membrane of giant liposomes (diameter 15–100 μm) by FtsA in the presence of Ficoll70³³. In their work, Furusato et al.³³ reported a homogenous recruitment of FtsZ to the membrane in the presence of FtsA but no membrane deformation. Local reshaping of liposomes was exclusively observed with ZapA as the FtsZ membrane anchor, but no constriction sites nor protein ring-like structures were observed³³. Here, we show that wild-type FtsA and FtsZ are capable to deform the membrane in PURE system-loaded liposomes with a size < 15 μm . The FtsA-dependent recruitment of FtsZ on the membrane frequently induces the formation of FtsZ clusters that constrict the liposome membrane into bud necks. It is clear from our data that FtsZ, assisted by FtsA, does not preferentially accommodate to pre-existing membrane areas with a high curvature. Conversely, membrane constriction and extended neck-like regions connecting the mother and budding vesicles are the product of localized FtsZ-FtsA pattern assembly. Noteworthy, these types of membrane remodeling, cytoskeletal protein organization, and dynamic blebbing structures were not observed in previous reports^{23,24,33,46}.

Not every liposome exhibits the same phenotype with regard to FtsZ recruitment and membrane deformation. This disparity is presumably the manifestation of the probabilistic encapsulation of all PURE system components and DNA, which leads to a large heterogeneity in FtsA expression levels, as recently quantified with a fluorescence reporter gene³⁵. It is therefore difficult to know the precise concentration of synthesized FtsA in individual liposomes and to correlate it with a particular phenotype.

Further investigations will be necessary for directing the assembly of an all-gene-based contractile FtsZ proto-ring that can divide liposomes. Although we do not exclude that assisting proteins, such as the Min system¹² and the FtsZ-interacting partners SlmA⁴⁷ and ZapB⁴⁸, might have to be introduced to complete membrane scission and release budding vesicles, the present results suggest that expression of FtsA and FtsZ might suffice to generate daughter vesicles of a few microns in size. The precise timing of protein interaction is essential for the hierarchical assembly of the proto-ring. This represents a major issue that is inherent to in-liposome compartmentalization of purified cytoskeletal proteins or with temporally unregulated expression of multiple genes. An additional level of temporal control that might be decisive for sequential assembly of the Z-ring constituents could be provided by regulating the expression of individual genes through transcriptional circuits, such as cascade or feedback motifs⁴⁹. Mindful of the limitations to apprehend the PURE system³⁴ and to rationally design liposomes harboring desirable properties encoded in genes, we believe that *in vitro* evolutionary optimization, by exploring a wide genetic diversity, provides additional opportunities to build cellular functions, and FtsZ proto-rings in particular.

Methods

DNA constructs. *ftsZ* and *ftsA* gene fragments were amplified by standard polymerase chain reaction (PCR) from the chromosomal *E. coli* BL21 DNA with primers 509 and 374 (*ftsZ*), and 508 and 376 (*ftsA*) (Supplementary Table 4). These primers contain overhangs for Gibson assembly with the pET11-a plasmid. PCR products were checked on a 1% agarose gel stained with EtBr or SYBR safe, imaged with a ChemiDoc™ Imaging System (BioRad Laboratories), and purified with the Wizard SV Gel kit (Promega). The purified DNA was incubated with DpnI (New England BioLabs®, Inc.) to remove residual plasmid and the linear DNA was purified again with Wizard SV Gel kit. DNA concentration and purity were measured using a ND-1000 UV-Vis Spectrophotometer (Nanodrop Technologies). Gibson assembly (Gibson Assembly® Master Mix of New England BioLabs®, Inc.) was performed at equimolar concentrations of linearized plasmid (pET11-a) and DNA fragments for 1 h at 50 °C. *E. coli* TOP10 competent cells (ThermoFisher Scientific, USA, catalog number C4040-10) were transformed with the Gibson assembly products by heat shock. Cells were centrifuged, resuspended in 50 μL of

fresh prechilled liquid lysogeny broth (LB) medium and incubated for 1 h at 37 °C and 250 rpm. The cultures were plated on solid LB medium with ampicillin and grew overnight at 37 °C. Colonies were picked up and cultured in 1 mL of liquid LB medium with 50 µg µL⁻¹ of ampicillin in 1.5-mL Eppendorf tubes for 6 h at 37 °C and 250 rpm. Plasmid purification was performed using the PureYield™ Plasmid Miniprep System (column method, Promega). Plasmid concentration and purity were checked on a Nanodrop. Linear templates for PURE system reactions were prepared by PCR using the plasmids as substrates with primers 194 and 709 (Supplementary Table 4). Amplification products were checked on a 1% agarose gel and were purified using the Wizard SV Gel kit. DNA concentration and purity were measured using a ND-1000 UV-Vis Spectrophotometer (Nanodrop Technologies).

The DNA fragment containing the *zapA* gene (original sequence from *E. coli* K12 strain) was inserted in a pIDTSMART-AMP plasmid (Integrated DNA Technologies). The plasmid was transformed into *E. coli* TOP10 cells. Transformation, plasmid purification, and production of linear DNA templates were performed as described above.

The *ftsA*_{opt} and *zapA*_{opt} constructs (starting with a T7 promoter and ending with the T7 terminator) were sequence-optimized for codon usage, GC content and 5' mRNA secondary structures, and were inserted in a pJET1 and pUC57 plasmid, respectively (GeneScript). Plasmids were amplified and purified as described above. All sequences of the linearized constructs can be found in the Supplementary Methods.

Purified proteins. Purified FtsZ and sZipA were prepared and labeled with Alexa Fluor probes according to published protocols^{24,50,51}. The degree of labeling was 0.9 ± 0.2 mol of fluorophore per mol of protein in both cases. FtsZ (150 µM) was dialyzed against 20 mM Hepes/HCl, pH 8.0, with 50 mM KCl, 5 mM MgCl₂, and 1 mM ethylenediaminetetraacetic acid (EDTA). To minimize perturbations on FtsZ assembly properties owing to labeling, the protein was first polymerized at 30 °C upon addition of 20 mM CaCl₂ and 2 mM GTP. A 20-fold excess of Alexa Fluor 647 (A647) was added, and the mixture was incubated for 15 min at 30 °C. The precipitate was resuspended on ice in 50 mM Tris/HCl, pH 7.4, with 100 mM KCl, and the free fluorescent probe was removed by gel filtration. ZipA (50 µM) was labeled by adding 10-fold excess of Alexa Fluor 488 (A488) during 15 min at room temperature in 20 mM Hepes/HCl, pH 8.0, with 50 mM KCl. Labeling reaction was stopped by the addition of a 1:100 dilution of 1 M Tris buffer. The unreacted probe was removed by gel filtration. FtsZ-A647 (45 µM stock) was stored in a buffer containing 50 mM Tris, 500 mM KCl, 5 mM MgCl₂ and 5% glycerol at pH 7.4. sZipA-A488 (14.33 µM stock) was stored in a buffer containing 50 mM Tris, 50 mM KCl, and 1 mM EDTA at pH 7.4.

Cell-free gene expression. PURE_{frex2.0} (GeneFrontier Corporation, Japan) was utilized following storing and handling instructions provided by the supplier. Linear DNA templates were used in single-gene expression assays at a final concentration of 5 nM. In co-expression experiments, both *ftsA*_{opt} and *zapA*_{opt} constructs were included at 5 nM and 10 nM, respectively, along with 1 µL of DnaK Mix (GeneFrontier Corporation). DnaK Mix consists of highly purified *E. coli* DnaK, DnaJ, and GrpE chaperone proteins. Reactions of 20 µL volume were carried out in test tubes for 3 h at 37 °C. When indicated, samples were supplemented with purified proteins (FtsZ-A647, sZipA-A488) and added either on top of an SLB or used for lipid film swelling.

QconCAT purification. QconCAT was designed to contain two specific peptides for FtsA and two for ZapA (Supplementary Table 1, Supplementary Fig. 2). QconCAT was expressed in BL21(DE3) cells in M9 medium with ¹⁵NH₄Cl and ampicillin. A pre-culture was diluted 1:100 to a 50-mL expression culture. Protein expression was induced at OD₆₀₀ = 0.5 with 1 mM isopropyl β-D-1-thiogalactopyranoside and cells were grown for 3 h at 37 °C. Cells were harvested by centrifugation and the pellet was dissolved in 1 mL B-PER. 10 µL of 10 mg mL⁻¹ lysozyme and 10 µL of DNaseI (ThermoScientific, 1 U µL⁻¹) were added and the sample was incubated for 10 min at room temperature. The lysate was centrifuged for 20 min at 16,000 × g and the pellet resuspended in 2 mL of a 1:10 dilution of B-PER in MilliQ water. The sample was twice again centrifuged, and the pellet was resuspended in 2 mL 1:10 diluted B-PER and centrifuged again. The pellet was resuspended in 600 µL of 10 mM Tris-HCl pH 8.0, 6 M guanidinium chloride and incubated at room temperature for 30 min. After spinning down unsolubilised protein the supernatant was loaded onto an equilibrated mini NiNTA spin column and the flow-through was reloaded twice to maximize protein binding. The column was washed twice with 600 µL of 10 mM Tris-HCl pH 6.3, 8 M urea and the QconCAT was eluted with 3 × 200 µL of 10 mM Tris-HCl pH 4.5, 8 M urea, 400 mM imidazole. The eluate was dialyzed overnight and for additional 4 h against 10 mM Tris-HCl pH 8.0, 100 mM KCl with a 10-kDa cutoff slide-a-lyzer cassette (ThermoScientific).

Trypsin digest. Per LC-MS injection, 1.5 µL of PURE system reaction was mixed with 3 µL of 100 mM Tris-HCl pH 8.0, 0.3 µL of 20 mM CaCl₂, and 0.8 µL MilliQ water. Samples were incubated at 90 °C for 10 min to stop the reaction. Then, 0.6 µL of QconCAT (0.3 mg mL⁻¹) was added, the sample was incubated again at 90 °C

for 10 min and after cooling to room temperature 0.3 µL of 1 mg mL⁻¹ trypsin (trypsin-ultra, MS-grade, New England Biolabs) was added. Samples were then incubated at 37 °C overnight. After addition of 0.7 µL 10% trifluoroacetic acid, samples were centrifuged in a table-top centrifuge (5415 R, Eppendorf) for 10 min at maximum speed. The supernatant was transferred to a glass vial with small-volume insert for LC-MS/MS analysis.

LC-MS/MS analysis. LC-MS/MS analysis was performed on a 6460 Triple Quad LCMS system (Agilent Technologies, USA) using Skyline software⁵². In all, 7 µL of sample was injected per run to an ACQUITY UPLC® Peptide CSH™ C18 Column (Waters Corporation, USA). The peptides were separated in a gradient of buffer A (25 mM formic acid in MilliQ water) and buffer B (50 mM formic acid in acetonitrile) at a flow rate of 500 µL per minute and at a column temperature of 40 °C. The column was equilibrated with 98% buffer A. After injection, the gradient was changed linearly over 20 min to 70% buffer A, over the next 4 min to 60% buffer A, and over the next 30 s to 20% buffer A. This ratio was held for another 30 s and the column was finally flushed with 98% buffer A to equilibrate for the next run. Selected peptides were measured by multiple reaction monitoring. For both ZapA and FtsA, two peptides were present in the QconCAT. In addition, two peptides from ribosomal proteins were also measured as control.

Labeling of in vitro synthesized proteins and gel analysis. PURE_{frex2.0} reaction mixtures were supplemented with 0.5 µL of GreenLys (FluoroTect™ GreenLys, Promega) and gene expression was performed in a test tube as described above. Samples were treated with RNase (RNaseA Solution, Promega) for 30 min and proteins were denatured for 10 min at 90 °C in 2× SDS loading buffer with 10 mM DTT. Samples were loaded on a 18% sodium dodecyl sulphate-polyacrylamide gel electrophoresis gel. Visualization of the fluorescently labeled translation products was performed on a fluorescence gel imager (Typhoon, Amersham Biosciences) using a 488-nm laser and a band pass emission filter of 520 nm.

Fabrication and cleaning of the imaging chambers. Home-made glass chambers were used in both SLB and liposome experiments¹². Three microscopy glass slides (1-mm thick) were glued on top of each other with NOA 61 glue (Norland Products) and holes with a diameter of 2.5 mm were drilled. A 150 µm-thick coverslip (Menzel-Gläser, Germany) was glued with NOA 61 to cover the apertures, creating the bottom of glass chambers. Cleaning was performed by successive washing steps of 10 min each in a bath sonicator (Sonorex digitec, Bandelin), as follows: chloroform and methanol (1:1 volume ratio), 2% Hellmanex, 1 M KOH, 100% ethanol and finally MilliQ water. For SLB experiments the glass chambers were further treated every two to three experiments with Acid Piranha.

Lipids. 1,2-dioleoyl-sn-glycero-3-phosphocholine (DOPC), 1,2-dioleoyl-sn-glycero-3-phosphoethanolamine (DOPE), 1,2-dioleoyl-sn-glycero-3-phosphoglycerol (DOPG), 1',3'-bis[1,2-dioleoyl-sn-glycero-3-phospho]-glycerol (18:1 CL), 1,2-distearoyl-sn-glycero-3-phosphoethanolamine-N-(biotinyl(polyethylene glycol)-2000 (DSPE-PEG-biotin), and 1,2-dioleoyl-sn-glycero-3-[(N-(5-amino-1-carboxypentyl)iminodiacetic acid)succinyl] (DGS-NTA) were from Avanti Polar Lipids. Texas Red 1,2-dihexadecanoyl-sn-glycero-3-phosphoethanolamine (DHPE-TexasRed) was from Invitrogen.

Preparation of small unilamellar vesicles. Small unilamellar vesicles (SUVs) were used as precursors for the formation of SLBs¹². Lipids DOPC (4 µmol), DOPG (1 µmol) and DGS-NTA (0.25 µmol), all dissolved in chloroform (Avanti Polar Lipids), were mixed in a glass vial. A lipid film was deposited on the wall of the vial upon solvent evaporation by applying a gentle flow of argon and was further desiccated for 30 min at room temperature. The lipid film was resuspended with 400 µL of SLB buffer (50 mM Tris, 300 mM KCl, 5 mM MgCl₂, pH 7.5) and the solution was vortexed for a few minutes. The final lipid concentration was 1.25 mg mL⁻¹. A two-step extrusion (each of 11 passages) was carried out using the Avanti mini extruder (Avanti Polar Lipids) equipped with 250 µL Hamilton syringes (Avanti Polar Lipids), filters (drain disc 10 mm diameter, Whatman) and a polycarbonate membrane with a pore size of 0.2 µm (step 1) or 0.03 µm (step 2) (Nuclepore track-etched membrane, Whatman).

Formation of SLBs. The imaging chamber was treated with oxygen plasma (Harrick Plasma basic plasma cleaner) for 30 min to activate the glass surface. Immediately after plasma cleaning the SUV solution was added to the sample reservoir at a final lipid concentration of 0.94 mg mL⁻¹ together with 3 mM CaCl₂. The chamber was closed by sticking a coverslip using a double-sided adhesive silicone sheet (Life Technologies) and the sample was incubated for 30 min at 37 °C. Next, the chamber was opened and the SLB was carefully washed six times with SLB buffer. Under these conditions, the SLB contains 4.8 molar % of 18:1 DGS-NTA (Ni²⁺) lipids, which is within the range studied by ref. ²⁷ (0.5–10 mol %), similar as in ref. ²⁸ (1–8 mol%) but higher than in ref. ³⁸ (0.02–0.08 mol% of full-length ZipA, DGS-NTA lipid was not used in this study) and lower than in ref. ⁵⁰ (10 mol%).

Activity assays on supported membranes. In the experiments involving sZipA-A488, 1 μM of the purified protein was first incubated on top of an SLB for 10 min at room temperature. The SLB was washed with 10 μL reaction buffer (50 mM Tris-HCl, 150 mM KCl, 5 mM MgCl_2 , pH 7.5). Then, 20 μL of sample (composition is specified where relevant) was added on top of the SLB and the chamber was sealed by sticking a 20×20 mm coverslip with a double-sided adhesive silicone sheet. In the experiments with FtsA, the *ftsA* or *ftsA_{opt}* gene was either directly expressed on top of the SLB, or in a test tube and subsequently added onto an SLB as part of the sample. In the earlier configuration, a 20 μL PURE_{frex2.0} reaction was carried out on top of an SLB and 10 μL were removed and replaced by the activity assay mixture. The exact composition of the sample varies for the different experiments and is specified where appropriate. In all cases, samples contained 2 mM GTP, supplemented with 2 mM ATP in FtsA experiments. In all assays without ZapA, Ficoll70 was added to a final concentration of 50 g L^{-1} . No oxygen-scavenging system was used, unlike in ref. 28 but like in ref. 38.

Spinning disk microscopy. SLBs were imaged with an Olympus iX81 inverted fluorescence microscope equipped with a $\times 100$ oil immersion objective (Olympus), an iXon3 EMCCD camera (Andor Technology) and a Nipkow spinning disk (CSU-XI, Yokogawa). FtsZ-A647 and sZipA-A488 were imaged using a 640 nm and 491 nm laser line, respectively, and appropriate emission filters (685/40 nm or 525/50 nm). The software Andor IQ3 (Andor Technology Ltd.) was used for image acquisition and identical settings were used for all experiments. Experiments were conducted at room temperature.

Preparation of lipid-coated beads. Lipid-coated beads were prepared according to our published protocol³⁵ with the following lipid composition: DOPC (50 mol%), DOPE (36 mol%), DOPG (12 mol%), 18:1 CL (2 mol%), DSPE-PEG-biotin (1 mass%) and DHPE-TexasRed (0.5 mass%) for a total mass of 2 mg. Lipids dissolved in chloroform were mixed in a round-bottom glass flask. Methanol containing 100 mM rhamnose (Sigma Aldrich) was added to the solution in a chloroform-to-methanol volume ratio of 2.5:1. Then, 1.5 g of 212–300 μm glass beads (acid washed, Sigma Aldrich) were poured to the lipid-rhamnose mixture and the organic solvent was removed by rotary evaporation at 200 mbar for 2 h at room temperature, followed by overnight desiccation. Lipid-coated beads were stored under argon at -20°C until use.

Production and immobilization of gene-expressing liposomes. A PURE_{frex2.0} reaction mixture was assembled as described above. Either or both *ftsA_{opt}* and *zapA_{opt}* DNA constructs were added at a final concentration of 5 nM and 10 nM, respectively. The solution was supplemented with (final concentrations indicated): 2 mM GTP, 2 mM ATP, 3 μM FtsZ-A647 and MilliQ to reach a final volume of 20 μL . About 20 mg of lipid-coated beads was added to the solution and liposomes were formed by natural swelling of the lipid film for 2 h on ice, protected from light. During incubation, the tube was gently rotated manually a few times. Four freeze-thaw cycles were then applied by dipping the sample in liquid nitrogen and thawing on ice. The sample reservoir of the imaging chamber was functionalized with 1:1 molar ratio of bovine serum albumin (BSA) and BSA-biotin (1 mg mL^{-1} , ThermoFisher Scientific), and then with Neutravidin (1 mg mL^{-1} , Sigma Aldrich), to tether the biotinylated liposomes. About 7 μL of the liposome solution was carefully pipetted (with a cut tip) into the imaging chamber and supplemented with RQ1 DNase (0.07 U μL^{-1}) to preclude gene expression outside liposomes. The chamber was sealed by sticking a 20×20 mm coverslip with a double-sided adhesive silicone sheet. Expression was performed directly on the confocal microscope at 37°C for 1.5–6 h.

Confocal microscopy. A Nikon A1R Laser scanning confocal microscope equipped with an SR Apo TIRF $\times 100$ oil immersion objective was used to image liposomes. The 561 nm and 640 nm laser lines were used in combination with appropriate emission filters to image the Texas Red membrane dye and FtsZ-A647, respectively. The software NIS (Nikon) was used for image acquisition and identical settings were used for all experiments. Samples were mounted on a temperature-controlled stage maintained at 37°C during imaging.

Fluorescence recovery after photobleaching. FRAP experiments were performed on an Olympus iX81 spinning disk microscope. Images were acquired using the following protocol: 10 frames every s, 10 frames every 250 ms, 10 frames every 2 s, 10 frames every 4 s. Analysis of the FRAP images was performed with ImageJ^{53,54} using the FRAP profiler plug-in. The intensity of a bleached region of interest (ROI, 29×29 pixels) was measured over time and normalized to the intensity of the surrounding (250×250 pixels area centered on the ROI) to correct for the bleaching that occurs during image acquisition. Fitting of the FRAP curves was generated in GraphPad Software Inc. using a one-phase exponential model. At least three FRAP measurements were performed in each sample analyzed.

Structured illumination microscopy (SIM). 3D SIM images have been acquired with a Nikon SIM microscope equipped with a Nikon $\times 100$ and 1.49 NA Apo TIRF

SR objective and a 640 nm laser line. The acquisition and reconstruction of the SIM images have been performed using the Nikon NIS element software. SIM raw data and their corresponding reconstructed images were quality-checked using the Fiji plug-in SIMcheck⁵⁵.

Total internal reflection fluorescence microscopy. FtsA-FtsZ ring dynamic was investigated using a Nikon TiE inverted fluorescence microscope equipped with an iLAS2 illumination system, a Plan Apo $\times 100$ oil immersion objective and a $2 \times$ Photometrics EMCCD Evolve Camera. The 640 nm laser line was used in combination with appropriate emission filters to image FtsZ-A647. MetaMorph[®] Microscopy Automation Software was used for image acquisition.

Quantitative image analysis. Image analysis was performed using Mathematica (Wolfram Research, version 11.3). All images were corrected for uneven illumination by applying a Gaussian filter with radius 70 pixels to each image, fitting a third-degree polynomial to the filtered image, and dividing the original image pixel-by-pixel with the fitted polynomial. To segment the filaments a ridge filter with $\sigma = 1$ was applied and the resulting image was binarized using morphological binarization with the default parameters. When needed this image was convolved with a Laplacian-of-Gaussian filter with radius two pixels and inverted (necessary for images with thin filaments). Filament thicknesses were calculated from this image as the distance of the centerline of filaments to the edge using the distance transform function. Branch point density and filament curvature were calculated after the thinning operation was applied to the segmented image. Curvatures were approximated at each pixel along the thinned filament with a distance larger than two pixels to the next branch point using Gaussian smoothing on the derivative functions. The image processing steps are illustrated in Supplementary Fig. 3.

Filament dynamic was analyzed by computing kymographs in MatLab version 2018a. A user-defined ellipse was overlaid on the ring-like structures of interest based on the first image of the movie and the boundary pixel intensities of all frames were extracted.

Statistics and reproducibility. All experiments reported in this study have been reproduced and similar results have been obtained. Microscopy images displayed in the main text figures are representative of the sample properties as analyzed from larger fields of view in at least three independent biological repeats.

Reporting summary. Further information on research design is available in the Nature Research Reporting Summary linked to this article.

Data availability

All data and custom codes generated during the current study are available from the corresponding author on reasonable request. Source data underlying the plots shown in Supplementary Figures are provided in Supplementary Data 1.

Received: 11 March 2020; Accepted: 1 September 2020;

Published online: 30 September 2020

References

- Shimizu, Y. et al. Cell-free translation reconstituted with purified components. *Nat. Biotechnol.* **19**, 751–755 (2001).
- Gros, J., Devbhandari, S. & Remus, D. Origin plasticity during budding yeast DNA replication in vitro. *EMBO J.* **33**, 621–636 (2014).
- Lee, K., Gallop, J. L., Rambani, K. & Kirschner, M. W. Self-Assembly of filopodia-like structures on supported lipid bilayers. *Science* **329**, 1341–1345 (2010).
- Vignaud, T., Blanchoin, L. & Théry, M. Directed cytoskeleton self-organization. *Trends Cell Biol.* **22**, 671–682 (2012).
- Nguyen, P. A. et al. Spatial organization of cytokinesis signaling reconstituted in a cell-free system. *Science* **346**, 244–247 (2014).
- Garner, E. C., Campbell, C. S., Weibel, D. B. & Mullins, R. D. Reconstitution of DNA segregation driven by assembly of a prokaryotic actin homolog. *Science* **315**, 1270–1274 (2007).
- Dannhauser, P. N. & Ungewickell, E. J. Reconstitution of clathrin-coated bud and vesicle formation with minimal components. *Nat. Cell Biol.* **14**, 634–639 (2012).
- Focus on the benefits of building life's systems from scratch. *Nature* **563**, 155–155 (2018).
- Nourian, Z., Scott, A. & Danelon, C. Toward the assembly of a minimal divisome. *Syst. Synth. Biol.* **8**, 237 (2014).
- Scott, A. et al. Cell-free phospholipid biosynthesis by gene-encoded enzymes reconstituted in liposomes. *PLoS ONE* **11**, e0163058 (2016).

11. van Nies, P. et al. Self-replication of DNA by its encoded proteins in liposome-based synthetic cells. *Nat. Commun.* **9**, 1583 (2018).
12. Godino, E. et al. De novo synthesized Min proteins drive oscillatory liposome deformation and regulate FtsA-FtsZ cytoskeletal patterns. *Nat. Commun.* **10**, 4969 (2019).
13. Bi, E. & Lutkenhaus, J. FtsZ ring structure associated with division in *Escherichia coli*. *Nature* **354**, 161–164 (1991).
14. Ma, X., Ehrhardt, D. W. & Margolin, W. Colocalization of cell division proteins FtsZ and FtsA to cytoskeletal structures in living *Escherichia coli* cells by using green fluorescent protein. *Proc. Natl. Acad. Sci.* **93**, 12998–13003 (1996).
15. Hale, C. A. & de Boer, P. A. Recruitment of ZipA to the septal ring of *Escherichia coli* is dependent on FtsZ and independent of FtsA. *J. Bacteriol.* **181**, 167–176 (1999).
16. Walker, B. E., Männik, J. & Mannik, J. Transient membrane-linked FtsZ assemblies precede Z-ring formation in *Escherichia coli*. *Curr. Biol.* **30**, 499–508 (2019).
17. de Boer, P., Crossley, R. & Rothfield, L. The essential bacterial cell-division protein FtsZ is a GTPase. *Nature* **359**, 254–256 (1992).
18. Mukherjee, A. & Lutkenhaus, J. Guanine nucleotide-dependent assembly of FtsZ into filaments. *J. Bacteriol.* **176**, 2754–2758 (1994).
19. Pichoff, S. & Lutkenhaus, J. Unique and overlapping roles for ZipA and FtsA in septal ring assembly in *Escherichia coli*. *EMBO J.* **21**, 685–693 (2002).
20. Pichoff, S. & Lutkenhaus, J. Tethering the Z ring to the membrane through a conserved membrane targeting sequence in FtsA. *Mol. Microbiol.* **55**, 1722–1734 (2005).
21. Hale, C. A. & de Boer, P. A. Direct binding of FtsZ to ZipA, an essential component of the septal ring structure that mediates cell division in *E. coli*. *Cell* **88**, 175–185 (1997).
22. Ortiz, C., Natale, P., Cueto, L. & Vicente, M. The keepers of the ring: regulators of FtsZ assembly. *FEMS Microbiol. Rev.* **40**, 57–67 (2016).
23. Osawa, M. & Erickson, H. P. Liposome division by a simple bacterial division machinery. *Proc. Natl. Acad. Sci. USA* **110**, 11000–11004 (2013).
24. Cabré, E. J. et al. Bacterial division proteins FtsZ and ZipA induce vesicle shrinkage and cell membrane invagination. *J. Biol. Chem.* **288**, 26625–26634 (2013).
25. Ramirez-Diaz, D. A. et al. Treadmilling analysis reveals new insights into dynamic FtsZ ring architecture. *PLOS Biol.* **16**, e2004845 (2018).
26. Krupka, M. et al. *Escherichia coli* FtsA forms lipid-bound minirings that antagonize lateral interactions between FtsZ protofilaments. *Nat. Commun.* **8**, 15957 (2017).
27. Krupka, M., Sobrinos-Sanguino, M., Jiménez, M., Rivas, G. & Margolin, W. *Escherichia coli* ZipA organizes FtsZ Polymers into dynamic ring-like protofilament structures. *MBio* **9**, e01008–18 (2018).
28. Loose, M. & Mitchison, T. J. The bacterial cell division proteins FtsA and FtsZ self-organize into dynamic cytoskeletal patterns. *Nat. Cell Biol.* **16**, 38–46 (2014).
29. Osawa, M., Anderson, D. E. & Erickson, H. P. Curved FtsZ protofilaments generate bending forces on liposome membranes. *EMBO J.* **28**, 3476–3484 (2009).
30. Swzedziak, P., Wang, Q., Bharat, T. A. M., Tsim, M. & Löwe, J. Architecture of the ring formed by the tubulin homologue FtsZ in bacterial cell division. *Elife* **3**, e04601 (2014).
31. Söderström, B. et al. Disassembly of the divisome in *Escherichia coli*: evidence that FtsZ dissociates before compartmentalization. *Mol. Microbiol.* **92**, 1–9 (2014).
32. Daley, D. O., Skoglund, U. & Söderström, B. FtsZ does not initiate membrane constriction at the onset of division. *Sci. Rep.* **6**, 33138 (2016).
33. Furusato, T. et al. De novo synthesis of basal bacterial cell division proteins FtsZ, FtsA, and ZipA inside giant vesicles. *ACS Synth. Biol.* **7**, 953–961 (2018).
34. Doerr, A. et al. Modelling cell-free RNA and protein synthesis with minimal systems. *Phys. Biol.* **16**, 025001 (2019).
35. Blanken, D., van Nies, P. & Danelon, C. Quantitative imaging of gene-expressing liposomes reveals rare favorable phenotypes. *Phys. Biol.* **16**, 045002 (2019).
36. Rueda, S., Vicente, M. & Mingorance, J. Concentration and assembly of the division ring proteins FtsZ, FtsA, and ZipA during the *Escherichia coli* cell cycle. *J. Bacteriol.* **185**, 3344–3351 (2003).
37. Caldas, P. et al. Cooperative ordering of treadmilling filaments in cytoskeletal networks of FtsZ and its crosslinker ZapA. *Nat. Commun.* **10**, 5744 (2019).
38. Martos, A. et al. FtsZ polymers tethered to the membrane by ZipA are susceptible to spatial regulation by Min waves. *Biophys. J.* **108**, 2371–2383 (2015).
39. Rivas, G., Alfonso, C., Jiménez, M., Monterroso, B. & Zorrilla, S. Macromolecular interactions of the bacterial division FtsZ protein: from quantitative biochemistry and crowding to reconstructing minimal divisomes in the test tube. *Biophys. Rev.* **5**, 63–77 (2013).
40. Small, E. et al. FtsZ Polymer-bundling by the *Escherichia coli* ZapA orthologue, YgfE, involves a conformational change in bound GTP. *J. Mol. Biol.* **369**, 210–221 (2007).
41. Martos, A. et al. Characterization of self-association and heteroassociation of bacterial cell division proteins FtsZ and ZipA in solution by composition gradient-static light scattering. *Biochemistry* **49**, 10780–10787 (2010).
42. Hernández-Rocamora, V. M. et al. Dynamic interaction of the *Escherichia coli* cell division ZipA and FtsZ proteins evidenced in nanodiscs. *J. Biol. Chem.* **287**, 30097–30104 (2012).
43. Osawa, M. & Erickson, H. P. Inside-out Z rings - constriction with and without GTP hydrolysis. *Mol. Microbiol.* **81**, 571–579 (2011).
44. Geissler, B., Elraheb, D. & Margolin, W. A gain-of-function mutation in ftsA bypasses the requirement for the essential cell division gene zipA in *Escherichia coli*. *Proc. Natl. Acad. Sci.* **100**, 4197–4202 (2003).
45. Pichoff, S., Shen, B., Sullivan, B. & Lutkenhaus, J. FtsA mutants impaired for self-interaction bypass ZipA suggesting a model in which FtsA's self-interaction competes with its ability to recruit downstream division proteins. *Mol. Microbiol.* **83**, 151–167 (2012).
46. Osawa, M., Anderson, D. E. & Erickson, H. P. Reconstitution of contractile FtsZ rings in liposomes. *Science* **320**, 792–794 (2008).
47. Cabré, E. J. et al. The nucleoid occlusion SlmA protein accelerates the disassembly of the FtsZ protein polymers without affecting their GTPase activity. *PLoS ONE* **10**, e0126434 (2015).
48. Monterroso, B. et al. The bacterial DNA binding protein MatP involved in linking the nucleoid terminal domain to the divisome at midcell interacts with lipid membranes. *MBio* **10**, e00376–19 (2019).
49. Noireaux, V., Bar-Ziv, R. & Libchaber, A. Principles of cell-free genetic circuit assembly. *Proc. Natl. Acad. Sci.* **100**, 12672–12677 (2003).
50. Mateos-Gil, P. et al. FtsZ polymers bound to lipid bilayers through ZipA form dynamic two dimensional networks. *Biochim. Biophys. Acta* **1818**, 806–813 (2012).
51. González, J. M. et al. Essential cell division protein FtsZ assembles into one monomer-thick ribbons under conditions resembling the crowded intracellular environment. *J. Biol. Chem.* **278**, 37664–37671 (2003).
52. MacLean, B. et al. Skyline: an open source document editor for creating and analyzing targeted proteomics experiments. *Bioinformatics* **26**, 966–968 (2010).
53. Schneider, C. A., Rasband, W. S. & Eliceiri, K. W. NIH Image to ImageJ: 25 years of image analysis. *Nat. Methods* **9**, 671–675 (2012).
54. Rueden, C. T. et al. ImageJ2: ImageJ for the next generation of scientific image data. *BMC Bioinformatics* **18**, 529 (2017).
55. Ball, G. et al. SIMcheck: a toolbox for successful super-resolution structured illumination microscopy. *Sci. Rep.* **5**, 15915 (2015).

Acknowledgements

We thank Jeremie Capoulade and Duco Blanken for assistance with fluorescence microscopy, and Zohreh Nourian, Sanne Wiersma, Maryse Karsten and Mona Mohseni Kabir for preliminary experiments. Microscopy measurements were performed at the Kavli Nanolab Imaging Center Delft. This work was financially supported by the Netherlands Organization for Scientific Research (NWO/OCW) through the 'BaSyC—Building a Synthetic Cell' Gravitation grant (024.003.019) and the FOM program no. 151, and by the Spanish government grant BFU2016-75471-C2-1-P.

Author contributions

C.D. conceived and supervised the research. E.G., J.N., and C.D. designed the experiments. E.G., J.N., A.D., and I.Z. performed the experiments. E.G., J.N., I.Z., A.D., and C.D. analyzed the data. C.D. and E.G. wrote the paper. M.J. and G.R. provided the purified FtsZ and sZipA proteins. All authors discussed the results and gave inputs on the manuscript.

Competing interests

The authors declare no competing interests.

Additional information

Supplementary information is available for this paper at <https://doi.org/10.1038/s42003-020-01258-9>.

Correspondence and requests for materials should be addressed to C.D.

Reprints and permission information is available at <http://www.nature.com/reprints>

Publisher's note Springer Nature remains neutral with regard to jurisdictional claims in published maps and institutional affiliations.



Open Access This article is licensed under a Creative Commons Attribution 4.0 International License, which permits use, sharing, adaptation, distribution and reproduction in any medium or format, as long as you give appropriate credit to the original author(s) and the source, provide a link to the Creative Commons license, and indicate if changes were made. The images or other third party material in this article are included in the article's Creative Commons license, unless indicated otherwise in a credit line to the material. If material is not included in the article's Creative Commons license and your intended use is not permitted by statutory regulation or exceeds the permitted use, you will need to obtain permission directly from the copyright holder. To view a copy of this license, visit <http://creativecommons.org/licenses/by/4.0/>.

© The Author(s) 2020